ORIGINAL RESEARCH

Silver-loaded nanotubular structures enhanced bactericidal efficiency of antibiotics with synergistic effect in vitro and in vivo

Na Xu,[1,2,]* Hao Cheng,[3,4,]* Jiangwen Xu,[1] Feng Li,[3] Biao Gao,[1] Zi Li,[3] Chenghao Gao,[3] Kaifu Huo,[5] Jijiang Fu,[1,2] Wei Xiong[3]

[1]The State Key Laboratory of Refractories and Metallurgy, School of Materials and Metallurgy, Wuhan University of Science and Technology, [2]Institute of Biology and Medicine, Wuhan University of Science and Technology, [3]Orthopaedic Department, Tongji Hospital, Tongji Medical College, Huazhong University of Science and Technology, Wuhan, People's Republic of China; [4]Biomaterials Innovation Research Center, Division of Biomedical Engineering, Department of Medicine, Brigham and Women's Hospital, Harvard Medical School, Boston, MA, USA; [5]Wuhan National Laboratory for Optoelectronics, Huazhong University of Science and Technology, Wuhan, People's Republic of China

*These authors contributed equally to this work

Correspondence: Jijiang Fu
The State Key Laboratory of Refractories and Metallurgy, School of Materials and Metallurgy, Wuhan University of Science and Technology, 947 Heping Road, 430081, Wuhan, People's Republic of China
Email fujijiang@wust.edu.cn

Wei Xiong
Orthopaedic Department, Tongji Hospital, Tongji Medical College, Huazhong University of Science and Technology, 1095 Jiefang Avenue, Wuhan 430030, People's Republic of China
Email xiongweitongji@gmail.com

Abstract: Antibiotic-resistant bacteria have become a major issue due to the long-term use and abuse of antibiotics in treatments in clinics. The combination therapy of antibiotics and silver (Ag) nanoparticles is an effective way of both enhancing the antibacterial effect and decreasing the usage of antibiotics. Although the method has been proved to be effective in vitro, no in vivo tests have been carried out at present. Herein, we described a combination therapy of local delivery of Ag and systemic antibiotics treatment in vitro in an infection model of rat. Ag nanoparticle-loaded TiO_2 nanotube (NT) arrays (Ag-NTs) were fabricated on titanium implants for a customized release of Ag ion. The antibacterial properties of silver combined with antibiotics vancomycin, rifampin, gentamicin, and levofloxacin, respectively, were tested in vitro by minimum inhibitory concentration (MIC) assay, disk diffusion assay, and antibiofilm formation test. Enhanced antibacterial activity of combination therapy was observed for all the chosen bacterial strains, including gram-negative *Escherichia coli* (ATCC 25922), gram-positive *Staphylococcus aureus* (ATCC 25923), and methicillin-resistant *Staphylococcus aureus* (MRSA; ATCC 33591 and ATCC 43300). Moreover, after a relative short (3 weeks) combinational treatment, animal experiments in vivo further proved the synergistic antibacterial effect by X-ray and histological and immunohistochemical analyses. These results demonstrated that the combination of Ag nanoparticles and antibiotics significantly enhanced the antibacterial effect both in vitro and in vivo through the synergistic effect. The strategy is promising for clinical application to reduce the usage of antibiotics and shorten the administration time of implant-associated infection.

Keywords: implant-associated infection, silver nanoparticles, TiO_2 nanotube, antibiotics, synergistic bactericidal activity

Introduction

Titanium (Ti) implant-associated bacterial infection remains as one of the most serious complications that could lead to implant failure and serious disabilities.[1–3] Treatment with antibiotics is the most regular strategy to prevent and cure implant-associated infection in clinics. However, antibiotic resistance and biofilm formation are challenging the drug efficiency, resulting in an extended antibiotic therapy than a usual 6-week antibiotic administration.[4] Although gram-positive *Staphylococcus aureus* remains as one of the main pathogens leading to implant infection, the emerging methicillin-resistant *Staphylococcus aureus* (MRSA) and gram-negative bacteria are making the scenario more complex. MRSA is resistant to all β-lactam antibiotics that share structural similarity with methicillin.[5,6] The treatment of gram-negative bacteria is challenging due to the exterior protective lipopolysaccharide membrane.[7] Drug-resistant bacteria is an increasing public health issue that has led to millions of deaths

every year because of the shortage of effective therapeutics to combat the resistant bacteria. The rising trend in drug resistance can be partially attributed to the long-term use of antibiotics, promoting the formation of new resistant bacteria through the process of evolutionary pressure.[8–10]

In addition, biofilm, a multiple bacteria structure embedded in a three-dimensional extracellular polymeric substance, is a physical barrier to antibiotic molecules and protects the bacteria present inside from the attack of antibiotics.[11,12] Compared to planktonic bacteria, an incredible 1,000-fold higher dosage of antibiotic is needed to kill bacteria inside the biofilm.[13] Furthermore, biofilm can supply a microenvironment stimulating the formation of new genetic mutant bacterial strains, which are highly drug resistant.[14] From the abovementioned perspectives, developing a highly efficient antibacterial therapy, simultaneously making resistant bacteria more vulnerable to antibiotics, and inhibiting biofilm formation are highly desired.

The combination of systemic antibiotics treatment and local site delivery of silver (Ag) is an attractive antibacterial therapy to address the challenge. Silver nanoparticles possess highly efficient antibacterial activity toward many species of bacteria, including gram-negative bacteria, gram-positive bacteria, and resistant strains, such as MRSA.[15,16] The antibacterial mechanism of Ag involves multiple processes: 1) disrupting the integrity of cell wall[14,17]; 2) inhibiting cell wall synthesis[18]; 3) binding to and damaging DNA[19,20]; 4) preventing protein translation;[21] and 5) forming reactive oxygen species (ROS).[22–24] Silver nanoparticles have been incorporated into nanostructures for the preparation of bactericidal surface and exhibited excellent antibacterial effect.[25,26] Several recent studies indicated that Ag nanoparticles could enhance the antibacterial effect of antibiotics, such as vancomycin, gentamicin, rifampicin, and levofloxacin.[27–31] The mechanism of the synergistic effect is complicated and varies with the type of antibiotics. For example, the destruction of cell wall by Ag nanoparticles or ions makes the antibiotic-resistant bacteria more sensitive to antibiotics.[28] However, most of the in vitro data could not guarantee the expected in vivo results, and the appropriate animal model has not been established to test the antibacterial effect.

The present study aimed to determine the synergistic antibacterial effect of antibiotics and Ag nanoparticles against various bacterial strains in vitro and in vivo. We combined the commonly used antibiotics and Ag nanoparticles with systemic test of the synergistic bactericidal effect against four bacteria species, including representative gram-negative *Escherichia coli* (ATCC25922), gram-positive *S. aureus*

(ATCC25923), and MRSA strains (ATCC33591 and ATCC43300). Less quantity of Ag nanoparticles was incorporated into TiO$_2$-nanotubes (NTs; Ag-NTs), which minimized the risk of toxicity due to high concentrations of Ag ion. An implant infection model was built in a rat to demonstrate the enhanced antibacterial efficiency in vivo. Combination of commonly used antibiotics and Ag-NTs delivery coating would be expected to expedite the synergistic bactericidal activity against both planktonic bacteria and biofilm in vitro and in vivo, allowing an enhanced antibacterial effect with reduced use of antibiotics and shorter administration time.

Materials and methods
Materials
Ti (99.8% pure) was purchased from Goodfellow Cambridge Limited (Huntingdon, UK). Methanol and ethylene glycol were obtained from Sinopharm Chemical Reagent Co., Ltd (Beijing, People's Republic of China). Ammonium fluoride (NH$_4$F) and silver nitrate (AgNO$_3$) were obtained from Aladdin (Shanghai, People's Republic of China). Tryptic soy broth (TSB) medium, standard antibiotics, and antibiotic sensitivity paper disk were supplied by the National Institutes of Food and Drug Control (Beijing, People's Republic of China). Ag nanoparticles with a size of 40 nm were purchased from Sigma-Aldrich Co. (St Louis, MO, USA).

Specimen preparation
The Ag-NT coating was fabricated following a previous method.[25] Ti foils (10×10×1 mm^3) and Ti rods (length: 12 mm, diameter: 0.8 mm) were prepared and polished by SiC sandpapers and then ultrasonically washed with acetone, ethanol, and distilled water sequentially. TiO$_2$-NT coating was fabricated on the Ti surface by electrochemical anodization. The anodization process was carried out in a two-electrode cell equipped with a direct current (DC) power supply (IT6834; ITECH, People's Republic of China). The Ti foil or rod was used as the anode electrode, and the graphite was used as the counter electrode. The electrolyte was prepared by ethylene glycol containing methanol (5 vol%) and distilled water (5 vol%). Anodization was run for 30 min at 60 V followed by ultrasonic washing. TiO$_2$-NT specimens were formed after annealing at 450°C for 120 min in air.

To prepare Ag-NTs, unannealed TiO$_2$-NTs were soaked in the AgNO$_3$ solution (1 mol·L^{-1}) for 10 min. After being rinsed with distilled water and air drying, the samples were irradiated with ultraviolet (UV) light by a high-pressure Hg lamp for 10 min. The whole process ended up with sequential ultrasonic cleaning and air drying. The samples were

sterilized for 30 min with the UV light for future antibacterial experiments.

Sample surface characterization

The surface topography of sample was characterized by field emission scanning electron microscopy (FESEM; FEI Nova 400 Nano) and transmission electron microscopy (TEM; Philips CM20). The surface chemical composition was analyzed by X-ray photoelectron spectroscopy (XPS; ESCALAB 250Xi, Thermo Fisher Scientific, Waltham, MA, USA) and energy-dispersive X-ray spectrometry (EDS; Tecnai).

Silver ion release

The Ag release from Ag-NTs was monitored as follows. The Ag-NTs were immersed in phosphate-buffered saline (PBS; 5 mL) in dark, and PBS was refreshed every 24 h. To determine the Ag release quantity at 1, 3, 7, 10, and 14 days, the PBS was analyzed by inductively coupled plasma atomic emission spectrometry (ICP-AES; IRIS Advantage ER/S) with a specific 328.1 nm emission line for Ag.

Minimum inhibitory concentration (MIC) and combination assay

Antibiotics such as vancomycin, rifampin, gentamicin, cefamandole, penicillin, levofloxacin, and clindamycin were used in the study. The antibacterial activities of standard antibiotics and Ag nanoparticles were tested against four bacterial strains, including a representative gram-negative *E. coli* (ATCC25922), gram-positive *S. aureus* (ATCC25923), and MRSA strains (ATCC33591 and ATCC43300). Susceptibility tests were carried out in 96-well microtiter plates using a standard twofold broth microdilution method of the antibacterial agents in TSB, following Clinical and Laboratory Standards Institute (CLSI 2013) guidelines. Briefly, bacterial cells were cultivated to midexponential phase at 37°C in the TSB medium under aerobic conditions. Aliquots of 100 µL of the bacterial cells were then seeded in the wells of a 96-well microtiter plate at a density of 1×10^6 cell·mL^{-1}. A total of 100 µL each of the serially diluted solutions of the bactericidal agent was then added to the bacterial cells (antibiotics or nano-Ag). The MIC assay was repeated five times. The MIC was defined as the lowest drug concentration of visible growth after overnight incubation at 37°C. The synergistic effects of Ag were also investigated using a checkerboard method by determination of the fractional inhibitory concentration index (FICI).[32] FICI was calculated as follows: FICI = MIC (antibiotic + Ag)/MIC (antibiotic) + MIC (Ag + antibiotic)/MIC (Ag). The synergistic effects were interpreted as follows: FICI <0.5 (synergy), 0.5≤ FICI <1 (partial synergy), FICI =1 (additive), 2≤ FICI <4 (indifferent), and 4≤ FICI (antagonism).

Disk diffusion assay

In disk diffusion assay, 10 µL bacterial suspension (1.5×10^8 colony-forming units [CFUs]·mL^{-1}) was evenly dispersed on Mueller-Hinton (M-H) plates. Standard antibiotic disks were then impregnated with 10 µL of prepared Ag solution (PBS solution with released Ag at day 1 in the silver release test). Both control disks (without Ag) and experimental disks (with Ag) were placed onto the M-H plates. The plates were incubated at 37°C under aerobic conditions for 24 h to observe zone inhibition diameter. The disk diffusion assay was processed in triplicate.

Antibiofilm formation ability assay

The antiadhesive and antibiofilm formation properties were examined by scanning electron microscopy (SEM; S-4800; Hitachi Ltd., Tokyo, Japan). The Ag-NT samples and different standard antibiotic disks were immersed in 1 mL bacteria suspension with 1.5×10^8 cells in TSB and cultured for 48 h at 37°C. Nonadherent bacteria were removed by gentle rinses with PBS for three times. The samples were subsequently fixed with glutaraldehyde solution (2.5% concentration) for 2 h at 4°C, and then, the samples were dehydrated in ethanol series (30%, 50%, 70%, 90%, and 100%). After that, the samples were soaked into amyl acetate solution for 1 h at ambient temperature to replace the ethanol and then freeze-dried. The adherent bacteria and biofilm formation on resultant samples were coated with Au in a sputter coater and imaged using SEM.

Animals and surgical procedures

The study used a total of 60 adult male Sprague Dawley rats (average weight: 150 g), supplied by the Laboratory Animal Center of Tongji Medical College, Huazhong University of Science and Technology. All surgeries were performed following the protocol approved by the ethics committee of animal experiments (Huazhong University of Science and Technology, permit number 20140918R). The experimental rats were treated following the Guide for the Care and Use of Laboratory Animals (8th edition). Sixty rats were equally divided into three groups: group I (antibiotics treatment), group II (Ag-NT implant), and group III (Ag-NT implant and antibiotics). Before surgery, the rats were anesthetized with 50 mg pentobarbital per kg body weight by intraperitoneal

injection. After shaving and sterilizing with povidone iodine, an incision was made across the left knee. Then, a sterilized syringe needle (external diameter: 0.8 mm) was used to drill a hole through the tibia plateau, from the proximal to the distal end. The exposed medullary cavity was injected into 100 μL bacteria suspension in TSB (ATCC43300, 1.5×10^8 CFUs·mL^{-1}). After bacteria inoculation, rod sample Ag-NTs were implanted into the medullary cavity in group II and group III rats. Burr hole of the tibia plateau was sealed with sterilized bone wax, and skin openings were sutured and sterilized.

During the recovery period from anesthesia and surgery, rats were kept in individual clean, dry, and comfortable cages. An intense and frequent observation was given to respiratory function, thermoregulation, cardiovascular function, and electrolyte and fluid balance by experienced personnel. After recovery from anesthesia, biological functions such as intake and elimination were monitored. Special attention was paid on the incision site for dehiscence and timely removal of skin suture. Both group I and group III rats were divided into four subgroups and treated with four different kinds of antibiotic treatments, respectively (rifampicin 1.5 mg every 24 h, vancomycin 15–20 mg·kg^{-1} every 12 h, gentamicin 5 mg·kg^{-1} every 24 h, and levofloxacin 12 mg·kg^{-1} every 24 h), by tail veil injection. The therapy ended after 3 weeks. The health status of rats including weight, body temperature, and vitality were monitored daily as the reference.[33]

In vivo radiology

X-ray examination (DirectView DR3000; Kodak) was performed 3 weeks after the primary surgery to assess longitudinal infection symptoms of the rats. Rats were anesthetized with the pentobarbital as carried out previously. X-ray parameter was chosen according to the human hand imaging parameter.

Histological and immunohistochemical analysis

All rats were euthanized (anesthesia with an overdose of pentobarbital) after 3 weeks. The left tibia was removed and separated and subsequently fixed in 4% paraformaldehyde solution for 12 h. Specimens were then incubated in ethylenediaminetetracetic acid (EDTA) and further embedded in paraffin. Then, sagittal sections (5 μm thick) were stained with hematoxylin and eosin (H&E). An indirect immunostaining technique based on a specific *S. aureus* monoclonal antibody (ab37644; Abcam plc, Cambridge, UK) was used for the in situ identification of *S. aureus*, and polymerized HRP-anti mouse/rabbit IgG (KIT-9901, IHC Kit) was added as the secondary antibody.

Statistical analysis

The assays were processed in triplicate, and the results were expressed as mean ± standard deviation. A one-way analysis of variance (ANOVA) and a Student–Newman–Keuls (SNK) post hoc test were used to determine statistical significance; $P<0.05$ was considered significant.

Results

Sample surface characterization

The surface microstructure of specimens obtained by anodization at 60 V for 30 min is shown in Figure 1A. The TiO$_2$-NTs formed by anodization had a typical NT structure. The SEM image and TEM image (Figure 1B and C) of Ag-NTs show that the Ag nanoparticles with a size of 20–40 nm are clearly loaded at the inner surface of NT arrays. In Figure 1D, Ti, O, and Ag are clearly shown in the EDS curve. The full XPS survey spectrum of Ag-NTs in Figure 1E illustrates the chemical components of sample surface. The signals of Ag, Ti, C, and O were all detected. The C signal in the XPS curve is believed to arise from adventitious contamination. Figure 1F presents the fine XPS spectrum of Ag3d. The peaks at 367.9 and 373.9 eV were in accordance with Ag3d5/2 and Ag3d3/2, respectively, which suggested the existence of metallic Ag. The abovementioned results indicated that the Ag nanoparticles were successfully loaded into the NT arrays.

Ag release

Figure 1G shows the release profile of Ag ion from Ag-NT sample. The contents of released Ag ion at 1, 3, 7, 10, and 14 days were detected by ICP-AES. The Ag content was 0.14±0.02 ppm on the first day, which decreased gradually after the first 3 days. The Ag concentration reached a plateau with a value of 0.06±0.01 ppm after 7 days and lasted as long as 14 days. The amount of released Ag ion is almost undetectable after 2 weeks.

MICs and combination assay

The MIC (column A and column B) and FICI (column C) were detected five times to evaluate the synergistic antibacterial effect of antibiotics and nanosilver (Table 1). Generally, as shown in column A, rifampin showed the most efficient antibacterial activity with a smallest MIC from 0.125 to 0.25 μg·mL^{-1} against all the four bacterial strains. Vancomycin showed a consistent MIC value of 1 μg·mL^{-1} for tested strains, while gentamicin presented with a 1–16 μg·mL^{-1} inhibitory concentration and was more effective to kill *E. coli*. However, *E. coli* with an MIC of
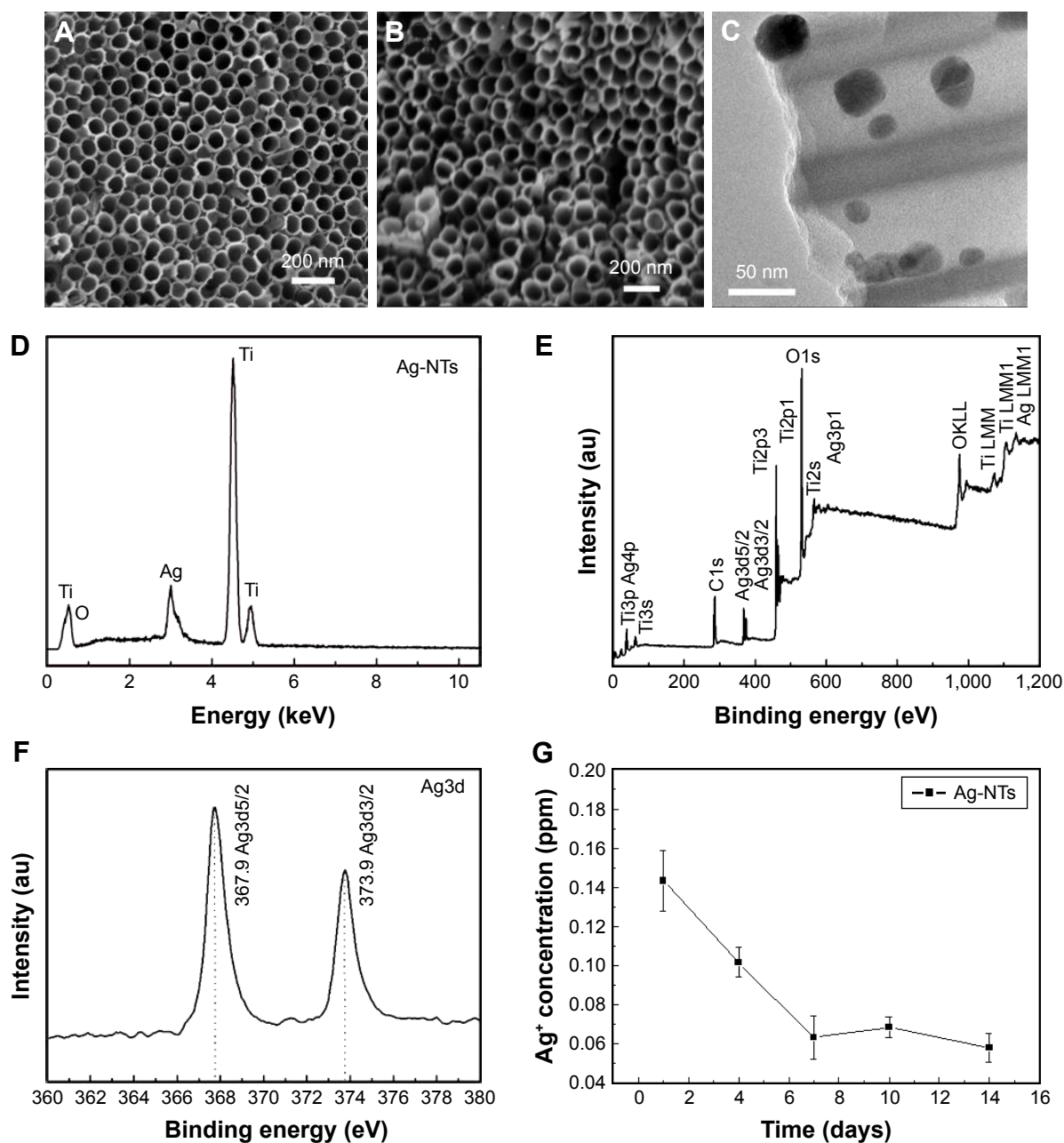
Figure 1 Surface characterization.
Notes: (**A**) and (**B**) are the SEM images of TiO$_2$-NTs and Ag-NTs, respectively. (**C**), (**D**), and (**E**) are the TEM image, EDS image, and full XPS spectrum of Ag-NTs, respectively. (**F**) is the fine XPS spectrum between 360 and 380 eV of Ag3d. The results prove that silver nanoparticles were successfully incorporated into the NT arrays. (**G**) is the noncumulative Ag release profile for 14 days from Ag-NTs into the PBS solution.
Abbreviations: SEM, scanning electron microscopy; NT, nanotube; TEM, transmission electron microscopy; EDS, energy-dispersive X-ray spectrometry; XPS, X-ray photoelectron spectroscopy; PBS, phosphate-buffered saline; au, astronomical unit.

0.25–2 µg·mL^{-1} was more sensitive to cefamandole compared to the other antibiotics. Higher MIC values were observed with levofloxacin 8–16 µg mL^{-1}, penicillin 16–128 µg mL^{-1}, and clindamycin 8–64 µg mL^{-1}. For Ag nanoparticles, the MIC value of all the four bacterial strains was in the range of 0.25–1 µg mL^{-1} with the smallest value observed for gram-negative *E. coli*. In Table 1 (column B), combinations of antibiotics and Ag nanoparticles resulted in a sharp decline

in MIC of the four strains, with 0.125–0.5 µg mL^{-1} for vancomycin, <0.125 µg·mL^{-1} for rifampin, 0.125–0.25 µg·mL^{-1} for gentamicin, 0.25–2 µg·mL^{-1} to 0.25–0.5 µg·mL^{-1} for cefamandole, 0.125–0.5 µg·mL^{-1} for penicillin, 0.125–0.5 µg·mL^{-1} for levofloxacin, and 0.25–0.5 µg·mL^{-1} for clindamycin. The FICI value (Table 1, column C) proved that vancomycin, rifampin, gentamicin, and levofloxacin showed synergistic (FICI <0.5) or partial synergistic (0.5≤ FICI <1)

Table I MIC assay and combination assay

Antibiotics	E. coli (ATCC 25922)				S. aureus (ATCC 25923)				MRSA (ATCC 33591)				MRSA (ATCC 43300)			
	A	B	C	P-value	A	B	C	P-value	A	B	C	P-value	A	B	C	P-value
Vancomycin	1	0.125	0.613 (PS)	<0.01	1	0.25	0.5 (PS)	<0.01	1	0.5	1	<0.01	1	0.125	0.375 (S)	<0.01
Rifampin	0.125	<0.125	1	<0.01	0.25	<0.125	<0.625 (PS)	<0.01	0.125	<0.125	0.25 (S)	<0.01	0.25	<0.125	<0.75 (PS)	<0.01
Gentamicin	1	0.125	0.625 (PS)	<0.01	2	0.25	0.325 (S)	<0.01	8	<0.125	0.15 (S)	<0.01	16	0.25	0.516 (PS)	<0.01
Cefamandole	0.25	0.125	1	<0.01	2	0.5	0.75 (PS)	<0.01	1	0.5	1.5	<0.01	1	0.5	1.5	<0.01
Penicillin	16	<0.125	0.5 (PS)	<0.01	32	0.5	0.516 (PS)	<0.01	>128	0.5	0.5 (S)	<0.01	>128	0.5	1	<0.01
Levofloxacin	16	0.125	0.508 (PS)	<0.01	16	0.5	0.532 (PS)	<0.01	8	0.5	0.563 (PS)	<0.01	16	0.25	0.516 (PS)	<0.01
Clindamycin	8	0.25	1.031	<0.01	16	0.5	0.532 (PS)	<0.01	32	0.5	0.516 (PS)	<0.01	64	0.5	1.008	<0.01
Nano-Ags	0.25				1				1				0.5			

Note: Columns A, B, C represent the MIC of antibiotics (µg·mL⁻¹), the MIC of antibiotics and silver nanoparticles (µg·mL⁻¹), and FICI, respectively.
Abbreviations: MIC, minimum inhibitory concentration; E. coli, Escherichia coli; S. aureus, Staphylococcus aureus; MRSA, methicillin-resistant Staphylococcus aureus; PS, partial synergistic; S, synergistic; FICI, fractional inhibitory concentration index.

effect on all the four chosen bacteria when combined with Ag nanoparticles.

Disk diffusion assay

The synergistic antibacterial activity of antibiotics and Ag was also analyzed by disk diffusion assay. Table 2 (column A) lists the inhibition zone diameter of 15.08–15.74 mm for vancomycin, 30.58–31.78 mm for rifampin, 10.00–11.84 mm for gentamicin, 15.57–24.33 mm for cefamandole, 9.74–19.87 mm for penicillin, 15.70–25.78 mm for levofloxacin, and 6.00–23.68 mm for clindamycin. In Table 2 (column B), a mild increase in the inhibition zone diameter could be observed in vancomycin and rifampin after being combined with silver (15.79–17.03 mm and 30.68–45.58 mm, respectively). A fold increase was measured in two groups (20.27–22.05 mm for gentamicin and 15.73–39.08 mm for penicillin), and a big increment was also observed (19.14–35.12 mm for cefamandole, 25.33–27.73 mm for levofloxacin, and 23.42–26.59 mm for clindamycin).

Antibiofilm formation ability assay

After 48 h incubation with 1 mL bacteria solution containing 1.5×10^8 bacteria cells, the samples were prepared for the SEM test. SEM images directly presented the biofilm formation on the surface of samples in Figure 2. Large quantity of CFUs stacked onto the surface of the TiO_2, and the two MRSA strains were more inclined to form biofilm. No typical biofilm formation was observed on Ag-NTs, and only a few separated bacteria colonies were able to be detected. When antibiotics vancomycin, rifampin, gentamicin, and levofloxacin were combined, respectively, few bacterial cells were found to adhere to the Ag-NT surfaces, including shrunken and broken down cells, which were regarded as dead cells.

In vivo radiology

After a 3-week antibiotic therapy, all the rats in group I (antibiotic) and group II (Ag-NTs) exhibited classic symptom of implant infection based on the results of X-ray examination in Figure 3. Bone absorption and periosteal reaction were evident, and extensive fibrosis of bone marrow cavity resulting from inflammatory response could also be observed. In contrast, the group III (Ag-NTs + antibiotic) rats showed no signs of infection.

Histological analysis and immunohistochemical analysis

The results of histological and immunohistochemical analyses are presented in Figures 4 and 5, respectively. In the H&E

Table 2 Disk diffusion assays

Antibiotics	E. coli (ATCC 25922)			S. aureus (ATCC 25923)			MRSA (ATCC 33591)			MRSA (ATCC 43300)		
	A	B	P-value	A	B	P-value	A	B	P-value	A	B	P-value
Vancomycin	15.08±1.54	16.05±1.75	<0.05	15.41±1.76	17.03±1.50	<0.05	15.50±1.43	15.79±1.90	<0.05	15.74±1.89	16.23±1.16	<0.05
Rifampin	30.58±2.95	32.43±4.09	<0.05	31.62±3.59	45.58±4.82	<0.01	30.65±2.78	30.68±3.71	<0.05	31.78±3.82	37.46±4.71	<0.01
Gentamicin	11.20±1.09	22.05±1.55	<0.05	10.00±1.12	21.28±1.76	<0.01	11.84±1.13	20.27±2.59	<0.01	10.00±1.25	21.89±3.55	<0.01
Cefamandole	18.65±1.43	35.12±4.12	<0.05	15.73±1.49	25.78±2.85	<0.05	15.57±1.89	19.14±1.56	<0.05	24.33±2.30	33.91±2.19	<0.01
Penicillin	15.24±1.84	39.08±2.87	<0.05	9.93±1.01	21.24±1.94	<0.01	9.74±0.86	15.73±1.69	<0.01	19.87±1.52	33.95±4.34	<0.01
Levofloxacin	25.78±2.73	27.57±2.77	<0.05	15.70±1.31	25.95±2.40	<0.01	25.46±2.60	27.73±2.43	<0.05	15.89±2.24	25.33±1.55	<0.01
Clindamycin	23.68±2.88	26.43±2.65	<0.05	6.00±0.75	23.42±0.45	<0.01	6.00±0.51	26.59±3.21	<0.01	6.00±0.58	25.44±2.29	<0.01

Note: Column A shows the inhibition zone diameter (mm) of standard antibiotics, and column B presents results of antibiotics and silver combination (mm).
Abbreviations: E. coli, Escherichia coli; S. aureus, Staphylococcus aureus; MRSA, methicillin-resistant Staphylococcus aureus.

staining results (Figure 4), group I (antibiotic) presented an abundant neutrophilic exudate and inflammatory cell infiltration accompanied with intramedullary necrosis and abscess, which provided the solid evidence of infection. Group II (Ag-NTs) rats showed a similar neutrophilic exudate and chronic inflammation response to group I samples. Group III (Ag-NTs + antibiotic) rats displayed no prominent inflammatory response and neutrophilic exudate. The immunohistochemical results in Figure 5 show that bacteria (ATCC 43300) were primarily located around the capillary loops and within the center of the inflammation and microabscesses in group I and group II. However, in group III, no bacteria were detected. The results further provided the presence of bacteria in group I and group II rats, which was consistent with the histological analysis staining.

Discussion

Preventive and therapeutic strategies have been extensively studied to decrease bacterial colonization and inhibit biofilm formation on surgically implanted materials, while systemic intravenous administration of antibiotics is still the first choice in clinics. Antibiotics are usually required to combat gram-negative MRSA and biofilm formation. However, the long-term use of antibiotics increased the risk of new antibiotic-resistant strain generation through the process of evolutionary pressure.[8–10,34] An alternative way to combat implant infection efficiently with a reduced antibiotics usage and shorter administration time is highly desired. Combination therapy of locally released Ag and systemic antibiotics treatment has been proved to be a considerable strategy due to their synergistic effect.[27–29]

Ag is generally considered biocompatible and safe at a low concentration[35–37]; hence, a local delivery platform offering controllable release property is in deep pursuit. TiO_2-NT coating has been proved to be a reservoir with efficient loading capacity for various nutrient elements, including Ag.[38,39] Our results shown in Figure 1 prove that, after hydrothermal treatment in the $AgNO_3$ solution, Ag nanoparticles with the size of 20–40 nm were incorporated into the inner wall of NTs. Compared to our previous studies,[25,26] a lower but sustaining release lasting for 2 weeks of Ag ion was observed. Considering the cytotoxicity of Ag, a smaller quantity of Ag ion is generally considered safer. An updated release pattern is detected because the depositing Ag amount was tuned by a lower immersing $AgNO_3$ concentration and soaking time compared to published studies.[25,26] In addition, Ag loading capacity can also be regulated with demandable TiO_2 inner diameter from 40 to 120 nm and various spatial distances between NTs.[40]
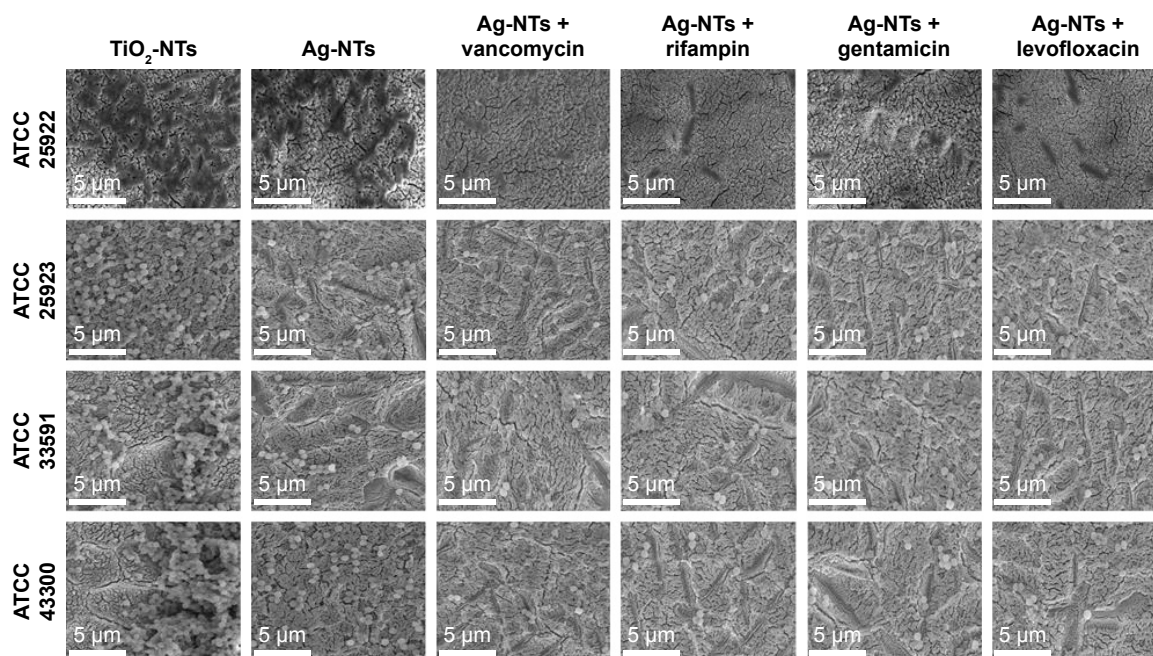
Figure 2 Antibiofilm formation characterization.
Notes: SEM images presented the inhibition ability of biofilm formation against bacterial strains ATCC 25923, ATCC 33591, ATCC 43300, ATCC 25922 on TiO₂-NTs, Ag-NTs, and Ag-NTs combined with antibiotics. A large quantity of colony-forming units stacked onto the surface of TiO₂ surface, and the two MRSA strains were more inclined to grow into biofilm formation. No typical biofilm formation was observed on Ag-NTs, and a few separated bacteria colonies were imaged. When added with antibiotics vancomycin, rifampin, gentamicin, or levofloxacin, only a few shrunken and broken bacteria cells were detected on the Ag-NT surfaces.
Abbreviations: SEM, scanning electron microscopy; NT, nanotube; MRSA, methicillin-resistant *Staphylococcus aureus*.

Here, we evaluated and demonstrated the combinational antibacterial properties of Ag-NT surfaces and seven commonly used antibiotics against four representative bacterial strains ATCC 25922 (*E. coli*), ATCC 25923 (*S. aureus*), ATCC 43300 (MRSA), and ATCC 33591 (MRSA) with MIC and combination assay, disk diffusion test, and antibiofilm formation ability test. In the present study, Table 1 clearly demonstrates that the Ag nanoparticle possessed smaller MIC against the four bacterial strains compared to all the used antibiotics except rifampin, especially when tested against gram-negative *E. coli*. After combination, the antibacterial activities of vancomycin, rifampin, gentamicin, and levofloxacin were increased to a synergistic or partial synergistic level. The highest enhancement of inhibition effect was observed with gentamicin against MRSA (ATCC 33591). More importantly, the two MRSA bacterial strains and gram-negative *E. coli* were found to be more sensitive to the combined therapy. Consistent with the abovementioned combination assay, the ZOI results in Table 2 further proved the enhanced antibacterial activity of antibiotics and Ag nanoparticles. After being impregnated with the Ag solution, all the antibiotic standard disks exemplified a bigger inhibition zone. The biggest increase in the inhibition zone was observed at the combination of Ag and gentamicin. In addition, the SEM results in Figure 2 show the enhancement of

the antiattachment properties of the combination treatment, even though the samples were incubated with a higher bacterial density and a longer incubation time compared to our previous study.[25] Though the Ag-NTs already repelled bacteria adhesion moderately, the combination therapy reduced bacterial binding to a degree of few possibilities of biofilm formation. After adding antibiotics, only a few single bacterial colonies were able to adhere onto the Ag-NT surfaces. Moreover, these colonies exhibited a shrunken state, which is usually regarded as dead or dying bacteria.[41] Therefore, all the abovementioned results are consistent proofs of synergistic effect presented by Ag and antibiotics, including vancomycin, rifampin, gentamicin, and levofloxacin.

The potential mechanisms of synergistic effect between Ag and antibiotics are considered to include attacking the same target, binding of monomers to the membrane, and stimulating bactericidal agent penetration[23,42–49] (Figure 6). Specifically, vancomycin kills bacteria by blocking the molecules called peptidoglycans, which reinforce the bacterial cell wall; this is also the target of Ag.[46,49] They both lyse the cell wall and increase the following penetration of bactericidal agents into the bacterium, resulting in a further intracellular killing. Gentamicin and Ag work together by denaturing the 30S ribosomal subunit of bacteria,[46] thus stopping protein translation that is necessary for survival
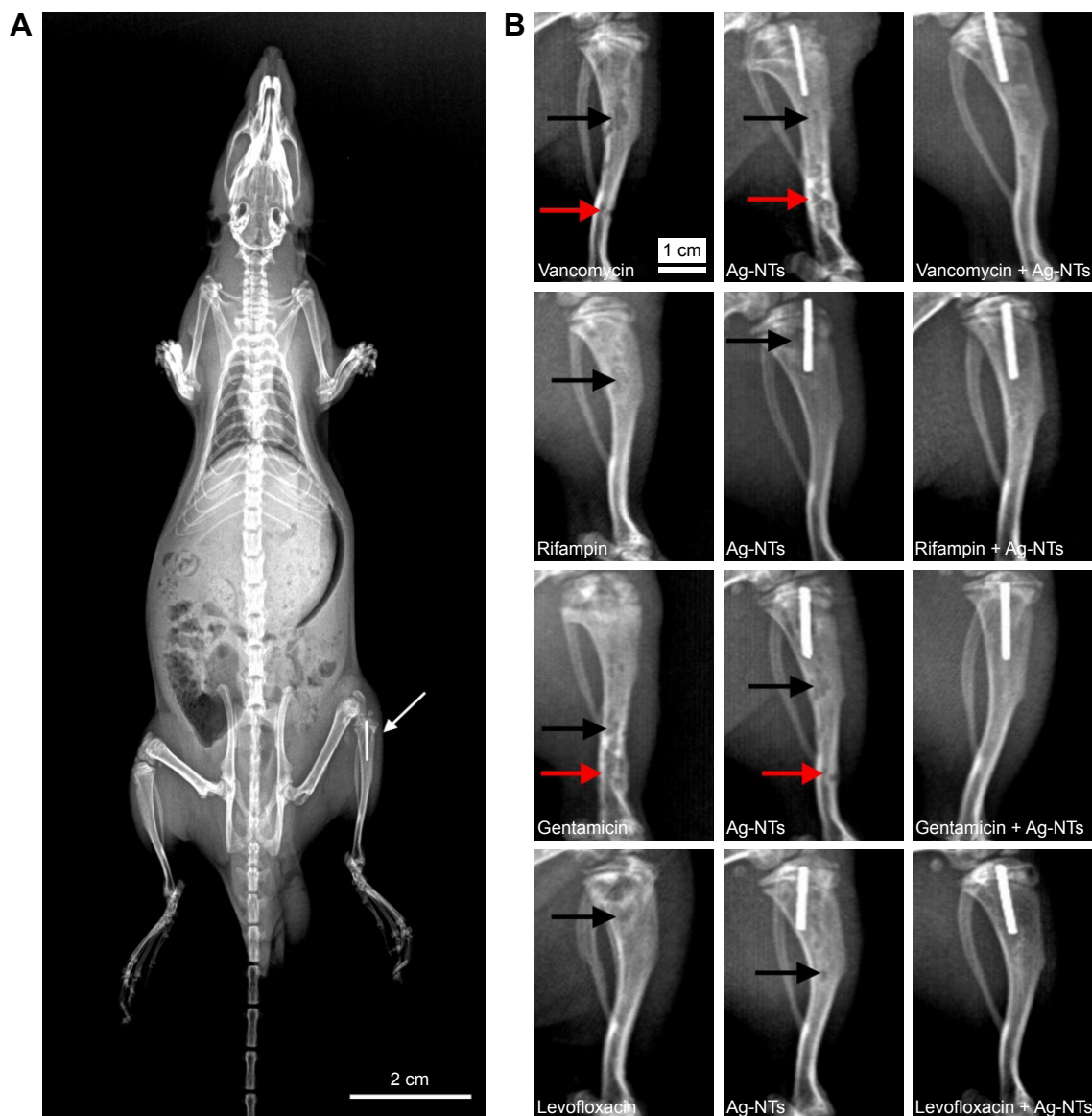
Figure 3 In vivo X-ray examination.
Notes: (**A**) X-ray examination of the bone implant infection model (male rats, 6 weeks old) implanted with Ti rods (white arrow) 1 h after surgery. (**B**) Images show X-ray examination 3 weeks post surgery. The rats in group I (antibiotic) and group II (Ag-NTs) exhibited classic symptoms of implant infection, including bone absorption (black arrow) and fibrosis (red arrow). The group III (Ag-NTs + antibiotic) rats showed no signs of infection.
Abbreviation: NT, nanotube.

of bacteria. In addition, gentamicin molecules contain many active groups such as amino and hydroxyl, which react easily with Ag nanoparticles by chelation.[29,50] The complex (Ag–gentamicin) may further bind to DNA, preventing DNA unwinding. Also, the Ag–gentamicin could potentially keep a more stable structure, thus potentially leading to a long-term antibacterial activity.[29] Rifampicin and levofloxacin kill bacteria by targeting their enzymes. By inactivating essential enzyme RNA polymerase, rifampicin blocks the transcription process. Levofloxacin inhibits the enzyme to impede the DNA replication and self-repair the bacteria.[43] The cell wall destruction caused by Ag helps rifampicin and

levofloxacin to enter the bacteria, which results in the rapid function loss of key enzymes. The enhanced antibiofilm formation activity is because of the blocking of biofilm formation process at the initial stage. Most bacteria were killed and inhibited during the swimming journey from culture medium to sample surfaces by Ag and antibiotics. Because of the released silver, the survival bacteria attached on the surface could hardly keep the integrity of cell wall, which is essential for the initial adhesion of the bacteria.[42,48] There may be some survivors, but the scattered residue bacteria can hardly continue to the next step of biofilm formation due to lack of quorum sensing.[45,47]
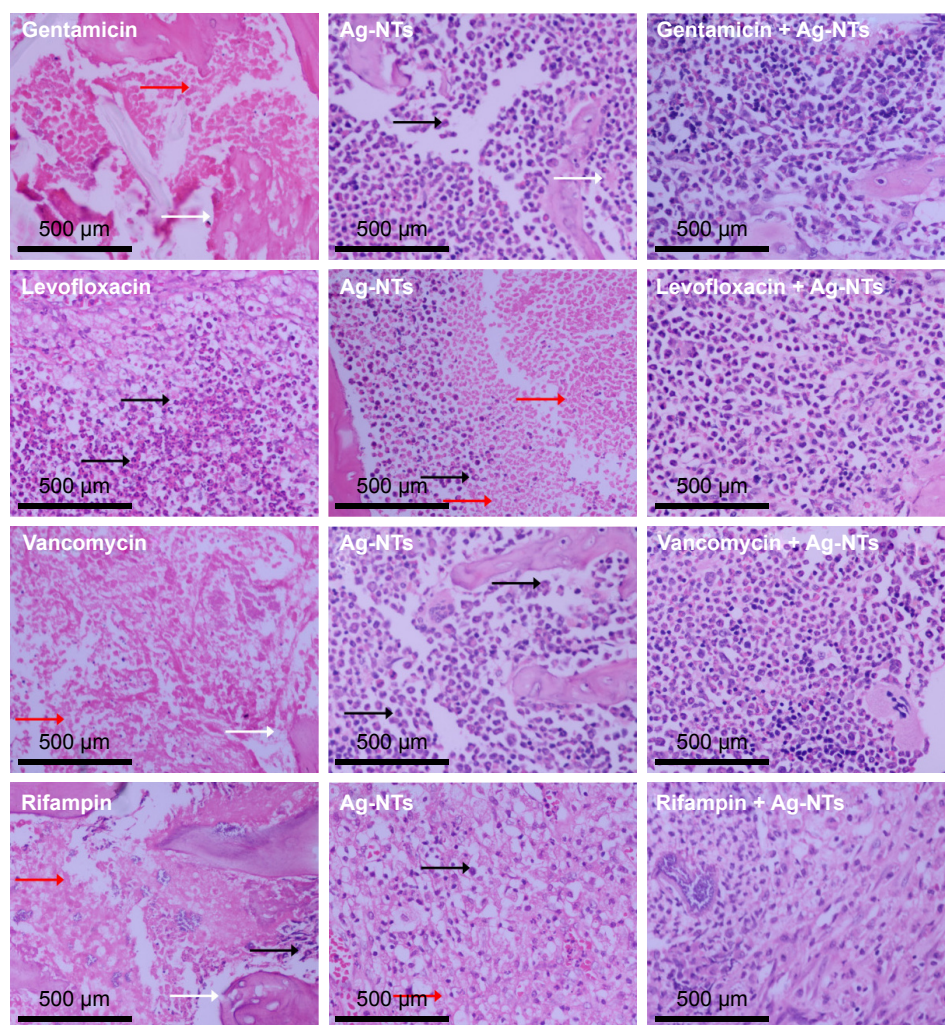
Figure 4 H&E staining for histological analysis.

Notes: Both group I (antibiotic) and group II (Ag-NTs) rats presented abundant neutrophilic exudate and inflammatory cell infiltration (black arrow) accompanied with intramedullary necrosis (white arrow) and abscess (red arrow), providing the evidence of infection. In group III (Ag-NTs + antibiotic), no prominent inflammatory response and neutrophilic exudate were detected.

Abbreviations: H&E, hematoxylin and eosin; NT, nanotube.

Previous studies have reported enhanced outcomes with a combination of Ag nanoparticles and antibiotics in vitro.[27–31] However, the synergistic antibacterial activity is rarely tested in vivo. In this regard, we built an implant infection model with MRSA (ATCC 43300) and treated it with the combinational antibacterial therapy for further verification of the in vitro results. The whole surgical process followed the protocol in our previous report,[26] while a much higher bacteria quantity was injected into the tibia bone cavity.

Rather than choosing a regular long-term antibiotic therapy (at least 6 weeks), which increases the risks of drug resistance, we adapt a 3-week administration therapy in the in vivo study. In Figure 3, X-ray examination of the group I and II rats exhibited bone deformities and clear signs of infection (bone absorption, periosteal reaction, and fibrosis) 3 weeks after surgery, whereas group III rats showed no

evidence of infection. The histological (Figure 4) and immunohistochemical (Figure 5) analyses illustrated supportive results to the radiology outcomes. In groups I and II, bone tissue around the implant manifested inflammatory cell infiltration, intramedullary necrosis, and abscess, accompanied with bacteria in colonies. This case was not observed for group III rats. The results from the animal model demonstrated that the released Ag from Ag-NT surfaces enhanced the bactericidal capability of vancomycin, rifampin, gentamicin, and levofloxacin in vivo.

Conclusion

We demonstrated an enhanced antibacterial effect of the combination of antibiotics (vancomycin, rifampin, gentamicin, and levofloxacin) and in situ released Ag in vitro and in vivo through the synergistic activity. A low but efficient Ag release
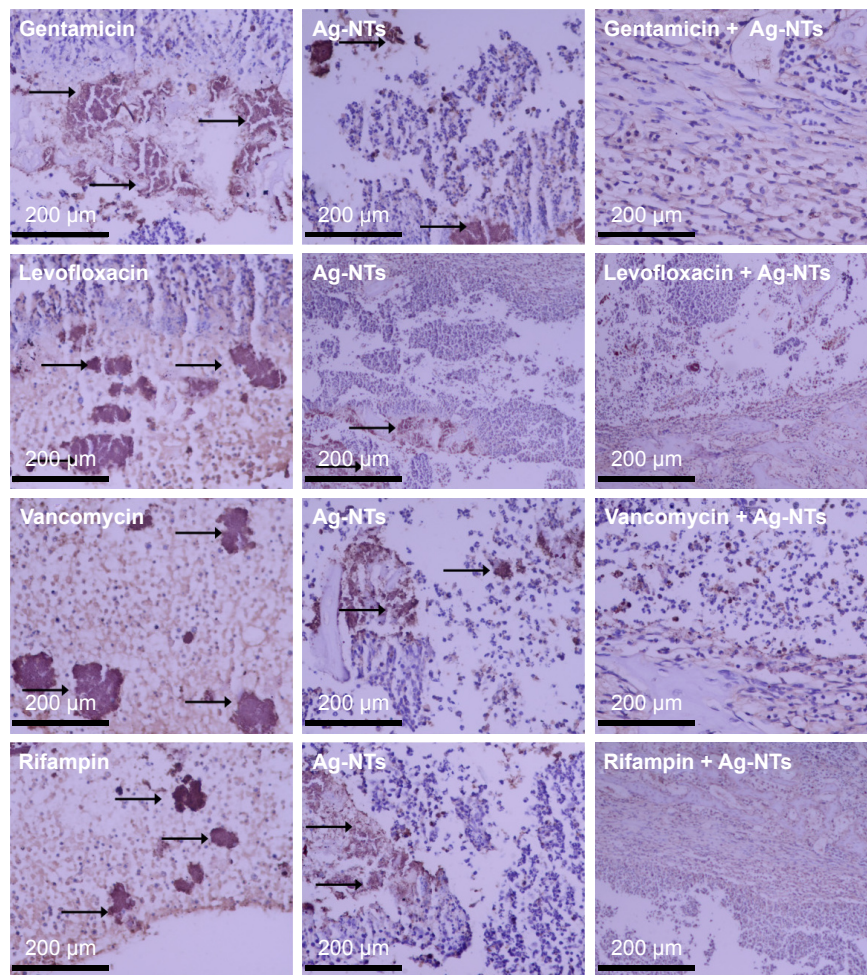
Figure 5 Immunohistochemical analysis.
Notes: In group I (antibiotic) and group II (Ag-NTs) rats, bacteria cells (ATCC 43300; black arrow) were located around the capillary loops or within the center of the inflammation and microabscesses. However, no bacteria were detected in group III (Ag-NTs + antibiotic).
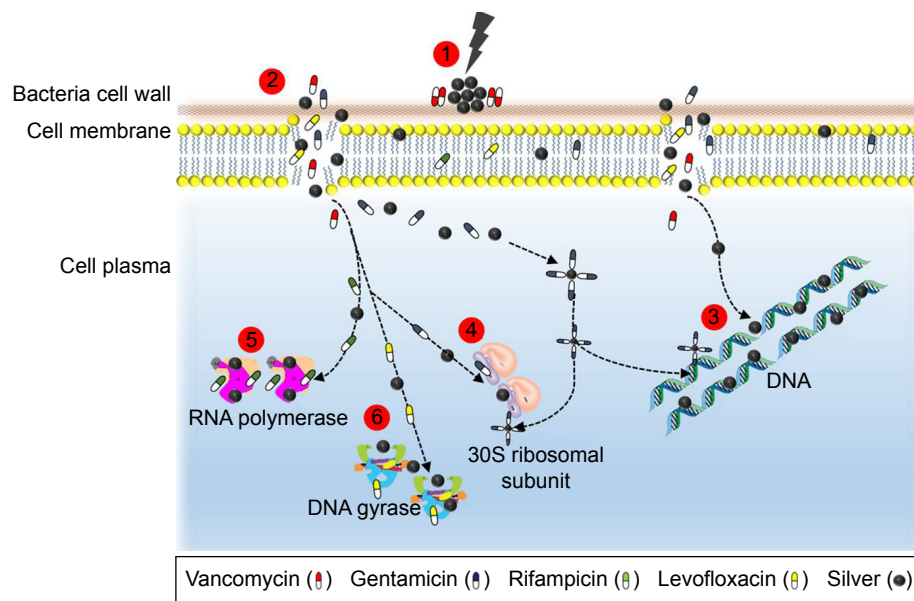**Abbreviation:** NT, nanotube.

Figure 6 The potential mechanism of synergistic effect between antibiotic and Ag: 1) lysing the cell wall; 2) stimulating the penetration of nano Ag into cell; 3) inactivating RNA polymerase; 4) denaturing 30S ribosomal subunit; 5) preventing DNA unwinding; and 6) inactivating DNA gyrase.

could be achieved from our designed Ag-NTs coating on Ti implants. The antibacterial effect was effective not only to wild-type *E. coli* (ATCC 25922) and *S. aureus* (ATCC 25923) but also to MRSA strains (ATCC 33591 and ATCC 43300). The combinational antibacterial therapy was further verified in vivo on an implant infection model. Our report proved that the combined application of Ag and antibiotics is an alternative to solve the problem of implant-associated infection and drug resistance.

Acknowledgments

Disclosure

The authors report no conflicts of interest in this work.

References

1. Cochis A, Azzimonti B, Della Valle C, Chiesa R, Arciola CR, Rimondini L. Biofilm formation on titanium implants counteracted by grafting gallium and silver ions. *J Biomed Mater Res A*. 2015;103(3):1176–1187.
2. Arciola CR, Campoccia D, Speziale P, Montanaro L, Costerton JW. Biofilm formation in *Staphylococcus* implant infections: a review of molecular mechanisms and implications for biofilm-resistant materials. *Biomaterials*. 2012;33(26):5967–5982.
3. Corvec S, Tafin UF, Betrisey B, Borens O, Trampuz A. Activities of fosfomycin, tigecycline, colistin, and gentamicin against extended-spectrum-β-lactamase-producing *Escherichia coli* in a foreign-body infection model. *Antimicrobl Agents Chemother*. 2013; 57(3):1421–1427.
4. Darley ES, MacGowan AP. Antibiotic treatment of gram-positive bone and joint infections. *J Antimicrob Chemother*. 2004;53(6):928–935.
5. Deurenberg RH, Vink C, Kalenic S, Friedrich AW, Bruggeman CA, Stobberingh EE. The molecular evolution of methicillin-resistant *Staphylococcus aureus*. *Clin Microbiol Infect*. 2007;13(3): 222–235.
6. Llarrull LI, Fisher JF, Mobashery S. Molecular basis and phenotype of methicillin resistance in *Staphylococcus aureus* and insights into new beta-lactams that meet the challenge. *Antimicrob Agents Chemother*. 2009;53(10):4051–4063.
7. Ellis TN, Leiman SA, Kuehn MJ. Naturally produced outer membrane vesicles from *Pseudomonas aeruginosa* elicit a potent innate immune response via combined sensing of both lipopolysaccharide and protein components. *Infect Immun*. 2010;78(9):3822–3831.
8. Palmer AC, Kishony R. Understanding, predicting and manipulating the genotypic evolution of antibiotic resistance. *Nat Rev Genet*. 2013;14(4):243–248.
9. Serisier DJ. Risks of population antimicrobial resistance associated with chronic macrolide use for inflammatory airway diseases. *Lancet Respir Med*. 2013;1(3):262–274.
10. Schaberle TF, Hack IM. Overcoming the current deadlock in antibiotic research. *Trends Microbiol*. 2014;22(4):165–167.
11. Pelgrift RY, Friedman AJ. Nanotechnology as a therapeutic tool to combat microbial resistance. *Adv Drug Deliv Rev*. 2013;65(13–14): 1803–1815.
12. Lebeaux D, Ghigo JM, Beloin C. Biofilm-related infections: bridging the gap between clinical management and fundamental aspects of recalcitrance toward antibiotics. *Microbiol Mol Biol Rev*. 2014;78(3): 510–543.
13. Sedlacek MJ, Walker C. Antibiotic resistance in an in vitro subgingival biofilm model. *Oral Microbiol Immunol*. 2007;22(5):333–339.
14. Nobile CJ, Mitchell AP. Genetics and genomics of *Candida albicans* biofilm formation. *Cell Microbiol*. 2006;8(9):1382–1391.
15. Stobie N, Duffy B, McCormack DE, et al. Prevention of *Staphylococcus epidermidis* biofilm formation using a low-temperature processed silver-doped phenyltriethoxysilane sol-gel coating. *Biomaterials*. 2008;29(8):963–969.
16. Knetsch ML, Koole LH. New strategies in the development of antimicrobial coatings: the example of increasing usage of silver and silver nanoparticles. *Polymers*. 2011;3:340–366.
17. Kim KJ, Sung WS, Suh BK, et al. Antifungal activity and mode of action of silver nano-particles on *Candida albicans*. *Biometals*. 2009;22(2): 235–242.
18. Sharma VK, Yngard RA, Lin Y. Silver nanoparticles: green synthesis and their antimicrobial activities. *Adv Colloid Iinterface Sci*. 2009;145(1–2): 83–96.
19. Rai M, Yadav A, Gade A. Silver nanoparticles as a new generation of antimicrobials. *Biotechnol Adv*. 2009;27(1):76–83.
20. Chaloupka K, Malam Y, Seifalian AM. Nanosilver as a new generation of nanoproduct in biomedical applications. *Trends Biotechnol*. 2010;28(11):580–588.
21. Rai M, Deshmukh S, Ingle A, Gade A. Silver nanoparticles: the powerful nanoweapon against multidrug-resistant bacteria. *J Appl Microbiol*. 2012;112(5):841–852.
22. Choi O, Hu Z. Size dependent and reactive oxygen species related nanosilver toxicity to nitrifying bacteria. *Environ Sci Technol*. 2008;42(12): 4583–4588.
23. Park HJ, Kim JY, Kim J, et al. Silver-ion-mediated reactive oxygen species generation affecting bactericidal activity. *Water Res*. 2009;43(4): 1027–1032.
24. Xu H, Qu F, Lai W, Andrew Wang Y, Aguilar ZP, Wei H. Role of reactive oxygen species in the antibacterial mechanism of silver nanoparticles on *Escherichia coli* O157:H7. *Biometals*. 2012;25(1):45–53.
25. Cheng H, Xiong W, Fang Z, et al. Strontium (Sr) and silver (Ag) loaded nanotubular structures with combined osteoinductive and antimicrobial activities. *Acta Biomater*. 2016;31:388–400.
26. Cheng H, Li Y, Huo K, Gao B, Xiong W. Long-lasting in vivo and in vitro antibacterial ability of nanostructured titania coating incorporated with silver nanoparticles. *J Biomed Mater Res A*. 2014;102A(10): 3488–3499.
27. Smekalova M, Aragon V, Panacek A, Prucek R, Zboril R, Kvitek L. Enhanced antibacterial effect of antibiotics in combination with silver nanoparticles against animal pathogens. *Vet J*. 2016;209:174–179.
28. Panacek A, Smékalová M, Rová RV, et al. Silver nanoparticles strongly enhance and restore bactericidal activity of inactive antibiotics against multiresistant Enterobacteriaceae. *Colloids Surf B Biointerfaces*. 2016;142:392–399.
29. Fayaz AM, Balaji K, Girilal M, Yadav R, Kalaichelvan PT, Venketesan R. Biogenic synthesis of silver nanoparticles and their synergistic effect with antibiotics: a study against gram-positive and gram-negative bacteria. *Nanomedicine*. 2010;6(1):103–109.
30. Hwang I-S, Hwang JH, Choi H, Kim K-J, Lee DG. Synergistic effects between silver nanoparticles and antibiotics and the mechanisms involved. *J Med Microbiol*. 2012;61(pt 12):1719–1726.
31. Gurunathan S. Biologically synthesized silver nanoparticles enhances antibiotic activity against Gram-negative bacteria. *J Ind Eng Chem*. 2015;29:217–226.
32. Orhan G, Bayram A, Zer Y, Balci I. Synergy tests by E test and checkerboard methods of antimicrobial combinations against *Brucella melitensis*. *J Clin Microbiol*. 2005;43(1):140–143.
33. Nicklas W, Baneux P, Boot R, et al. Recommendations for the health monitoring of rodent and rabbit colonies in breeding and experimental units. *Lab Anim*. 2002;36(1):20–42.

34. Harms MJ, Thornton JW. Evolutionary biochemistry: revealing the historical and physical causes of protein properties. *Nat Rev Genet*. 2013;14(8):559–571.

35. Acosta-Torres LS, Mendieta I, Nunez-Anita RE, Cajero-Juarez M, Castano VM. Cytocompatible antifungal acrylic resin containing silver nanoparticles for dentures. *Int J Nanomedicine*. 2012;7:4777–4786.

36. de Lima R, Seabra AB, Duran N. Silver nanoparticles: a brief review of cytotoxicity and genotoxicity of chemically and biogenically synthesized nanoparticles. *J Appl Toxicol*. 2012;32(11):867–879.

37. Wu K, Yang Y, Zhang Y, Deng J, Lin C. Antimicrobial activity and cytocompatibility of silver nanoparticles coated catheters via a biomimetic surface functionalization strategy. *Int J Nanomedicine*. 2015;10:7241–7252.

38. Popat KC, Eltgroth M, LaTempa TJ, Grimes CA, Desai TA. Titania nanotubes: a novel platform for drug-eluting coatings for medical implants? *Small*. 2007;3(11):1878–1881.

39. Huo KF, Gao B, Fu JJ, Zhao LZ, Chu PK. Fabrication, modification, and biomedical applications of anodized TiO2 nanotube arrays. *RSC Adv*. 2014;4:17300–17324.

40. Li Y, Li F, Zhang C, et al. The dimension of titania nanotubes influences implant success for osteoclastogenesis and osteogenesis patients. *J Nanosci Nanotechnol*. 2015;15(6):4136–4142.

41. Wu PG, Imlay JA, Shang JK. Mechanism of *Escherichia coli* inactivation on palladium-modified nitrogen-doped titanium dioxide. *Biomaterials*. 2010;31(29):7526–7533.

42. van Loosdrecht MC, Lyklema J, Norde W, Zehnder AJ. Bacterial adhesion: a physicochemical approach. *Microb Ecol*. 1989;17(1):1–15.

43. Takei M, Fukuda H, Kishii R, Hosaka M. Target preference of 15 quinolones against *Staphylococcus aureus*, based on antibacterial activities and target inhibition. *Antimicrob Agents Chemother*. 2001;45(12):3544–3547.

44. Davies D. Understanding biofilm resistance to antibacterial agents. *Nat Rev Drug Discov*. 2003;2(2):114–122.

45. Hammer BK, Bassler BL. Quorum sensing controls biofilm formation in Vibrio cholerae. *Mol Microbiol*. 2003;50(1):101–104.

46. Liou GF, Yoshizawa S, Courvalin P, Galimand M. Aminoglycoside resistance by ArmA-mediated ribosomal 16S methylation in human bacterial pathogens. *J Mol Biol*. 2006;359(2):358–364.

47. Waters CM, Lu W, Rabinowitz JD, Bassler BL. Quorum sensing controls biofilm formation in Vibrio cholerae through modulation of cyclic di-GMP levels and repression of vpsT. *J Bacteriol*. 2008;190(7):2527–2536.

48. Hori K, Matsumoto S. Bacterial adhesion: from mechanism to control. *Biochem Eng J*. 2010;48:424–434.

49. Kohanski MA, Dwyer DJ, Collins JJ. How antibiotics kill bacteria: from targets to networks. *Nat Rev Microbiol*. 2010;8(6):423–435.

50. Wang YW, Tang H, Wu D, et al. Enhanced bactericidal toxicity of silver nanoparticles by the antibiotic gentamicin. *Environ Sci-Nano*. 2016;3:788–798.

→ Video abstract

Point your SmartPhone at the code above. If you have a QR code reader the video abstract will appear. Or use:

http://youtu.be/fY46GganJuY